Volume 16 | Number 13 | 7 April 2018 | Pages 2189–2364

Organic & Biomolecular Chemistry

rsc.li/obc

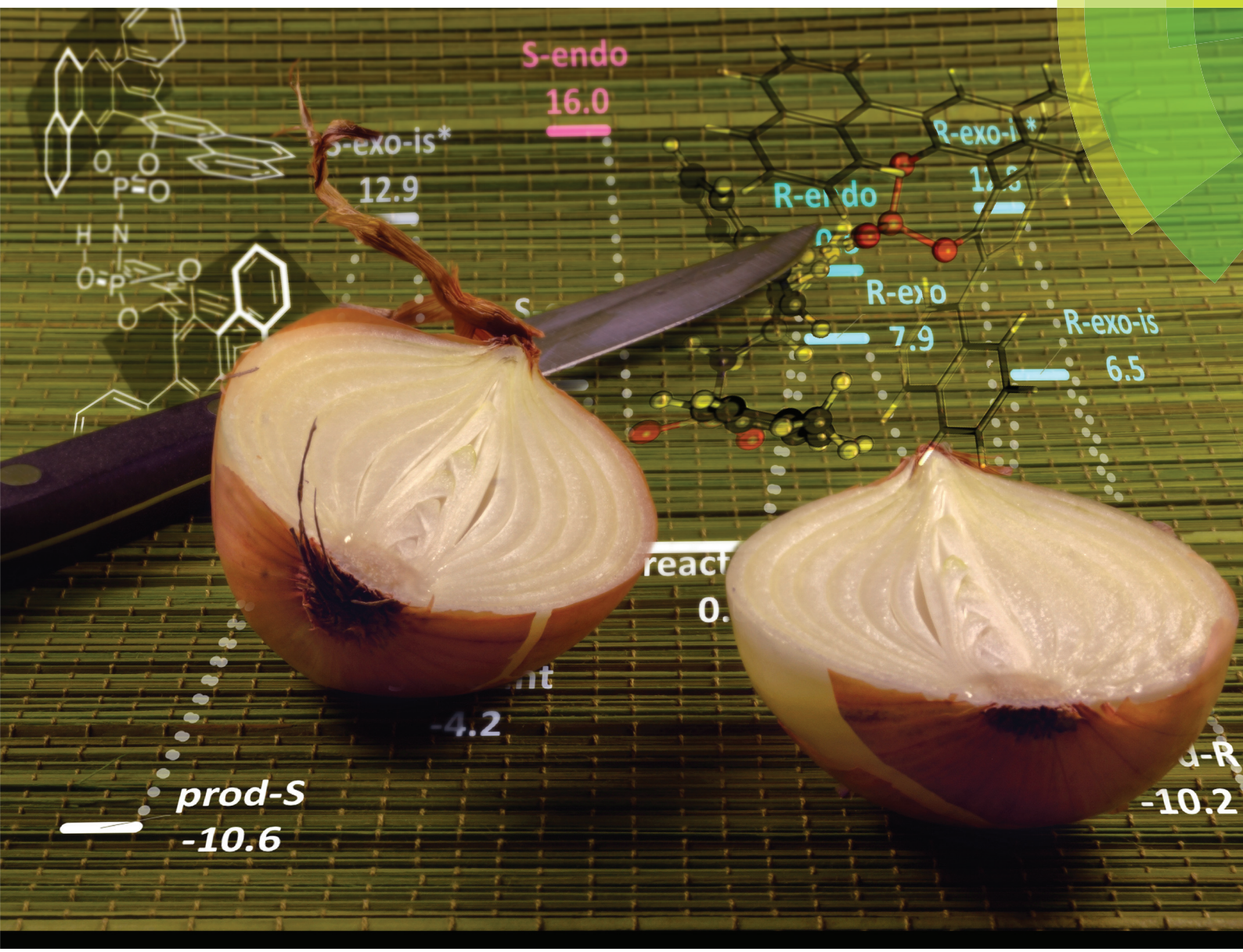

ISSN 1477-0520

ROYAL SOCIETY OF CHEMISTRY

PAPER
Luis Simón
Enantioselectivity in CPA-catalyzed Friedel–Crafts reaction of indole and *N*-tosylimines: a challenge for guiding models

Organic & Biomolecular Chemistry

PAPER

View Article Online
View Journal | View Issue

Cite this: *Org. Biomol. Chem.*, 2018, **16**, 2225

Enantioselectivity in CPA-catalyzed Friedel–Crafts reaction of indole and *N*-tosylimines: a challenge for guiding models†

Luis Simón

Received 22nd November 2017,
Accepted 24th January 2018

DOI: 10.1039/c7ob02875j

rsc.li/obc

Qualitative reaction models or predicting guides are a very useful outcome of theoretical investigations of organocatalytic reaction mechanism that allow forecasting of the degree and sense of the enantioselectivity of reactions involving novel substrates. However, application of these models can be unexpectedly challenging in reactions affected by a large number of conformations and potential control of the enantioselectivity by different reaction steps. The QM/MM study of the Friedel–Crafts reaction between indole and the *N*-tosylimide of benzaldehyde catalysed by different CPA reveals that the reaction consists of two CPA-assisted steps: the addition of the two reagents to yield a Wheland intermediate, and its re-aromatization. The relevance of the second step depends on the catalyst: it changes the sense of the expected stereoselectivity for a BINOP-derived CPA but is irrelevant in the reaction catalysed by a VAPOL-derived imidodiphosphoric acid catalyst. Although the relative energies of the TSs can be rationalized considering the steric interactions with the catalyst, the possibility of additional H-bonds, or the relative stability of the conformation of the reagents, predicting the enantioselectivity is not possible using qualitative guides.

Introduction

The availability of powerful computers and the development of reliable methodologies[1–3] have increased the utility of computational chemistry in catalysis.[4–6] On one side, computational chemistry can assist in deciphering the mechanism of the reaction and the different roles of the catalyst,[4,7] with important implications in improving the catalyst design. On the other side, the study of the details of the mechanism offers models for predicting the outcome of selective catalytic reactions. These models are valuable guides to choosing the right catalysts or designing synthetic routes that could profit from the selectivity. Citing only some examples in organocatalysis, we can consider: the Houk model for proline-catalysed aldol reactions,[8–10] the Jørgensen model for his own catalyst,[11] the Pápai model for bifunctional organocatalysts,[12,13] Grayson and Houk's model for conjugate additions catalysed by cinchona alkaloids,[14–16] Guo and Wong's model for cinchona alkaloid-squaramide catalysts,[17] Wu and Ding model for TADDOL catalysed Diels–Alder reactions,[18] *etc*.[7]

Chiral phosphoric acid (CPA) catalysts, whose popularity has recently seen rapid development,[19–28] constitute a good example of this two-fold contribution of computational chemistry to catalysis. Initial studies showed that CPA catalysts operate through a "*proton relay*" mechanism, making use of their bifunctional character.[29–37] From these studies, qualitative models have been formulated[37–46] that can lead the way to the right choice of substrates or catalyst.[47–49] The large number of applications of these catalysts has allowed these models to be tested against a large number of reactions (the Goodman model has been applied to more than 1000 transformations[48]); the commercial availability of different alternatives[24] also contributes to make these models more useful.

Friedel–Crafts reactions of indole are useful procedures for the preparation of compounds of interest.[50–55] CPA has been used on some of these reactions;[56–75] in particular, the reaction with the *N*-tosyl imine of benzaldehyde has been studied using BINOP-derived catalysts,[70] SPINOL-derived phosphates,[71,72] and imidodiphosphoric acid-derived catalysts,[69] showing different degrees of enantioselectivity. The reaction requires two steps: the formation of a new C–C bond, in which a new chiral centre is formed, and the re-aromatization of the intermediate. Mechanistic studies have shown that the latter step could be rate determining for some catalysed reactions of indole.[76] The availability of experimental results for different catalysts, the possibility of several rate-determining or stereo-

Facultad de Ciencias Químicas, Universidad de Salamanca, Plaza de los Caídos 1-5, Salamanca E37004, Spain. E-mail: lsimon@usal.es

†Electronic supplementary information (ESI) available. See DOI: 10.1039/c7ob02875j

determining steps in the reaction mechanism, and the flexibility of the *N*-tosyl imine reagent make this reaction a very attractive test case for the employment of qualitative prediction models.

In this paper, the mechanisms of several CPA-catalysed Friedel–Crafts additions of indole to the *N*-tosyl imine of benzaldehyde are studied by QM/MM methods. The calculations reproduce the experimental enantioselectivities, ensuring that the assumptions and methods used during the calculations are correct. The different competing transition state structures (TSs) are examined to deduce the origin of their differential stability. In addition, the possibility of reaching similar conclusions using simple guides inspired by qualitative models, without needing tedious calculations, is discussed.

For this study, the catalyst substituted with 1-naphthyl groups in the 3,3′ positions was chosen among other BINOP phosphoric acids used for this reaction[70] (Fig. 1a, **Cat I**). Each of the 1-naphthyl groups can pose two different orientations, yielding $2^2 = 4$ possibilities and increasing the computational effort. However, other simpler catalysts were discarded for this study since they require considerably longer reaction times to offer even smaller reaction yields. Modelling of slower reactions could be more troublesome since the experimental results could be more easily affected by the presence of traces of other catalysts or by side reactions that preferentially consume one of the enantiomers. For simplicity, only the energy and structures of the more stable TSs are discussed, although contributions from all calculated structures were considered for the calculation of the enantiomeric excesses (these TSs are shown in the ESI† section). From the SPINOL derived CPA alternatives,[71] 3,5-bis-(trifluoromethyl)-phenyl substituted (**Cat II**, Fig. 1b) was used, also considering that the reaction is faster with this catalyst.

As representatives of imidodiphosphoric acid catalysts,[69] a BINOP-type (**Cat III**, Fig. 1c) and a VAPOL-type (**Cat IV**, Fig. 1d) catalyst were studied. The BINOP-type catalyst is substituted with phenyl groups; the 1-naphthyl-substituted catalyst offers a slightly better yield, but the presence of four asymmetric 1-naphthyl groups would lead to $2^4 = 16$ possibilities, which constitutes a prohibitive increase of the computational effort. In addition, the phenyl-substituted catalyst yields a 90% ee, compared to 99% ee by the 1-naphthyl-substituted catalyst. Although the latter result is obviously more attractive, from a theoretical perspective a study of a less selective catalyst is more interesting: it is less likely that a wrong mechanism or inappropriate methodology could accidentally reproduce the experimental results. Remarkably, a mistake in the absolute configuration assignment of the major product with both imidodiphosphoric acid catalysts was discovered. Comparison of the sign of the rotatory power and retention times for identical chiral chromatography columns described in the literature[70,71,77] revealed that these catalysts yield the *S* enantiomer as the major product. To facilitate the discussion, all catalysts correspond to the *R* absolute configuration except for the SPINOL-derived catalyst, which shows *S* absolute configuration. Note, however, that *S*-SPINOL is structurally and stereochemically equivalent to *R*-BINOP.

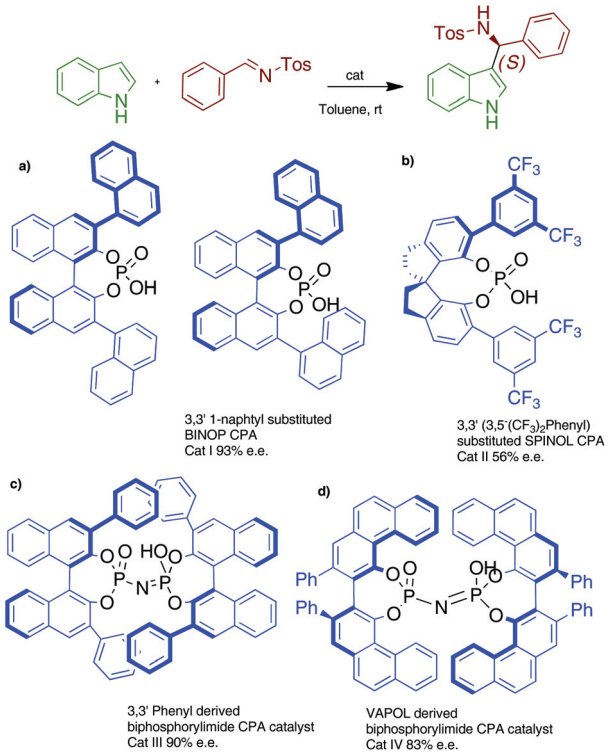

Fig. 1 Reaction and different organocatalysts studied. For **Cat I** two of the four possible alternative conformations of the 1-naphthyl groups are shown.

Computational methods

All calculations were performed using *Gaussian 09*.[78] The large number of atoms in the system, particularly for **Cat III** and **Cat IV**, and the degrees of freedom of the catalyst and reactants, make the use of pure QM calculations unreasonable. Fortunately, QM : MM ONIOM[79–81] hybrid methods offer reasonable agreement between experimental and theoretical results in studies[29,32,33,38,82–87] with similar or related organocatalysts. These methods require only a small fraction of the computational effort needed for pure QM methods. Only those atoms that participate in bond forming/breaking events or in establishing H-bond interactions were included in the high-level layer and were treated by a QM method: the atoms on both reagents and the phosphate group of the catalysts. The rest of the atoms of the catalysts were included in the low-level layer and were studied by a MM method. These atoms interact with the atoms in the QM layer through van der Waals interactions, which can be efficiently modelled by the Lenard-Jones potential included in the MM force fields.[5] The distribution of the atoms in the different layers is shown in 3D representations of the TSs by using a "*ball and stick*" representation for atoms in the QM layer and a wireframe representation for atoms in the MM layer. In Fig. 1, catalyst atoms in the MM layer are drawn in blue. 3D representations were rendered using Pymol[88] software.

During optimization and TSs searches, the B3LYP hybrid-GGA functional with the 6-31G(d,p)[89,90] basis set was used for the QM layer. This functional gives comparable TS geometries to meta-GGA functionals.[1] The low level layer was treated with a UFF[91] force field. Following the procedure used in the literature, the single-point energy of the optimized structure was then calculated using the QM method for the complete system. The ω-B97XD functional[92] and 6-311+G(d,p) basis set were used in this calculation. This functional includes explicit dispersion corrections that are important to reproduce the interactions between the catalyst and the reagents. Solvation effects for toluene were introduced in the single-point calculations using an implicit IEFPCM[93–97] procedure with the SMD[98] solvation model, with solvent-accessible surface cavities.

The thermal contribution to Gibbs free energy was calculated using the ONIOM(B3LYP/6-31G(d,p):UFF) frequencies since this analysis is only valid on structures that are stationary points at the level of theory used. The vibrational contribution to entropy was calculated using a quasi-rigid-rotor-harmonic-oscillator model using the method of Grimme[99] implemented in GoodVibes program,[100] which uses a free-rotor model for modes with frequencies smaller than a threshold (set to 100 cm^{-1}). Scale factors for harmonic frequencies were also used: the weights assigned in the Gaussian 09 output to the contribution of the layers for each vibrating mode were used to average the scale factor to 0.96 (indicated for B3LYP/6-31G(d,p)[101]) for atoms in the QM B3LYP and 0.87 for atoms in the MM layer. The 0.87 scale factor was derived from comparison of experimental and UFF frequencies for benzene, naphthalene and biphenyl (see details in ESI†). Gibbs free energy differences, used in the discussion, are calculated after adding to the ω-B97XD single-point energy the Gibbs free energy correction. Enantiomeric excesses were calculated assuming the Curtin–Hammett principle and using the Maxwell–Boltzmann populations at 298.15 K.

For some of the TSs, the relative energy of the conformation of the intermediate is used in the discussion. This energy was obtained after re-optimizing the intermediate structure once the catalyst atoms were removed, using the ω-B97XD/6-311+G(d,p) level of theory. The dihedral angle between the Hydrogen atoms at C3 and C1′ was restrained to the nearest *gauche* (±60°) or *anti* (180°) conformation.

Results and discussion

The reaction consists of two steps. First, the addition of the two reagents yields an indelium intermediate. This intermediate, also known as the Wheland intermediate, isomerizes in the second step to recover the aromaticity lost in the addition step, after losing the H atom on C3.

During the addition step, the reagents can show *endo* or *exo* relative orientations, depending on whether the imine nitrogen atom is over the indole ring or not. The indole can also approach the tosylamide on either the *re* or *si* face. The reaction can therefore yield four possible diastereomeric Wheland intermediates and four possible reaction paths. During the re-aromatization step, the chirality developed by the indole C3′ is lost (this carbon atom is planar in the products). Therefore, each product enantiomer can be generated by two of the different routes: the *R* product from either the *R-endo* or *R-exo* paths, and the *S* product from the *S-endo* or *S-exo* paths. The four possible routes are shown in Fig. 2 (note the change in the Ingold–Prelog priority rules from the Wheland intermedi-

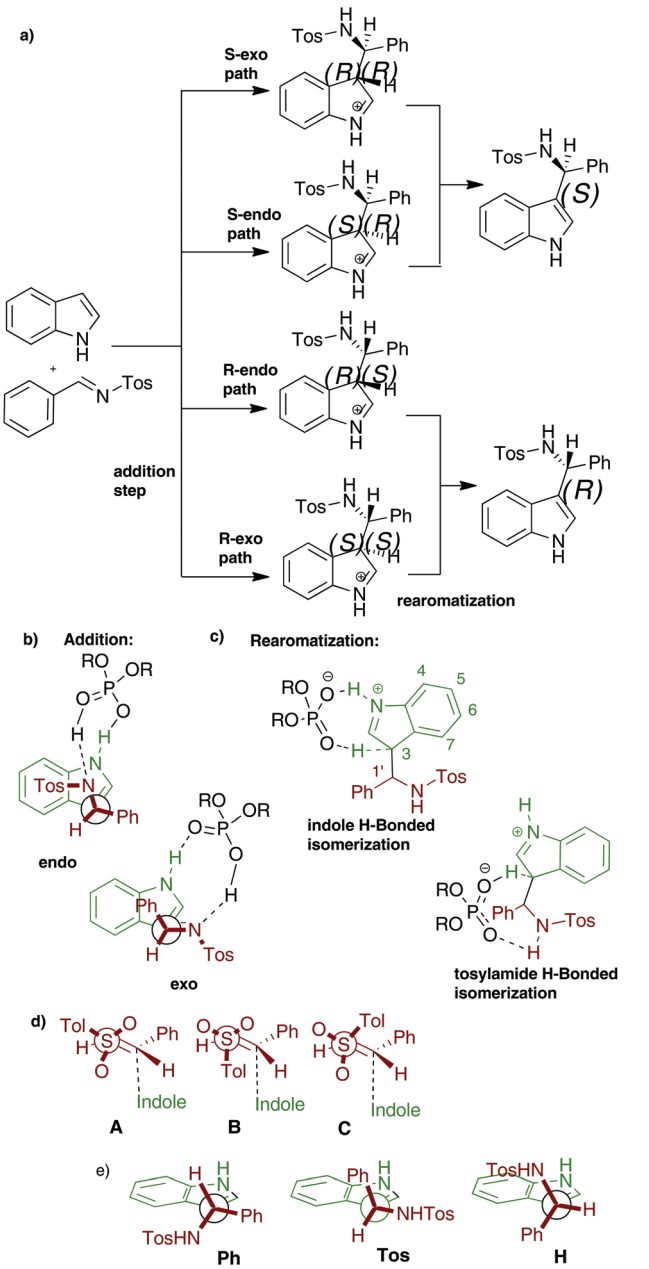

Fig. 2 (a) Different paths for the Friedel–Crafts reaction of indole with tosylimide of benzaldehyde; (b) *endo* and *exo* relative orientation of the reagents for the addition step; (c) isomerization TSs; (d) different conformations of the N–S bond; and (e) different conformations of the C3–C1 bond.

ates to the products; for simplicity, each route is labeled according to the absolute configuration of the final product).

Based on the literature precedents,[29–37] the CPA catalyst is considered to act during the addition step by establishing simultaneous interactions with both reagents (Fig. 2b). In the *exo* paths, three different conformations of the S–N bond are possible: one in which the aromatic ring is *anti* with respect to the C1′ (**A** in Fig. 2d), and two *gauche* conformations (**B** and **C**). For addition TSs in the *endo* paths, in *gauche* **B** conformation the tosyl group would be put toward the indole ring, so only the conformations **A** and **C** are considered. For simplicity, only the most stable of these conformations is discussed, although all TSs are used to calculate the stereoselectivity and are included in the ESI† section.

Next, the isomerization step is catalysed by the anion of the CPA catalyst. One of the phosphate oxygen atoms deprotonates the indolium C3 atom. The other oxygen can be H-bonded to either the indolium NH or the tosylamide NH, yielding two possible mechanisms: "*indole H-bonded*" and "*tosylamide H-bonded*" (Fig. 2c). For "*tosylamide H-bonded*" TSs, the H-bond between the CPA and the N′ atom fixes the C1′–C3 conformation, but for "*indole H-bonded*" TSs there are three possible conformations of this bond (Fig. 2e, named according to which of the H-, Ph- or Tos- groups is *syn-periplanar* to the indole C2–C3 bond). Three possible conformations of the C1′–C3 bond were also considered, although for simplicity only the most stable TSs is discussed. The energies of all TSs conformations were used to calculate the selectivity and all TSs are shown in the ESI† section.

For explaining and predicting the enantioselectivities of each step, different models were considered. The Goodman[39] model was used in the addition step with **Cat-I** and **Cat-II** (Fig. 3a). This model is based on a zenithal projection of the catalyst and the identification of hindered regions (to the left at the top and to the right at the bottom) and less sterically demanding regions (right at the top and left at the bottom). It offers similar results to the Himo–Terada[30,102] model, which is based on the identification of four quadrants in a frontal representation of the catalyst (Fig. 3a). For *R*-BINOP-derived catalysts the top-right and bottom-left (represented by gray boxes in Fig. 3a, **6**, **7**, **9** and **10**) quadrants are hindered. The advantage of the Goodman model is that the reagents are placed parallel (instead of oblique) to the paper and therefore it is easier to draw and use. This argument also points to the employment of the Himo–Terada model instead of the Goodman model in the isomerization step with these catalysts.

For **Cat-III** and **Cat-IV** the Simón and Paton[85] model for "confined" Brønsted acid catalysts was used (Fig. 3b and c). This model is based on a frontal representation of the catalyst's active site. For **Cat-III**, this projection reveals that the active phosphate oxygen atoms are buried in a cavity formed by two of the catalyst side phenyl groups (dark-gray boxes, Fig. 3b) that is also partially delimited at the top and the bottom by the other two phenyl groups (light-gray bars, Fig. 3b) situated behind. For **Cat-IV** the cavity is limited laterally by two of the phenanthryl groups but not at the top and

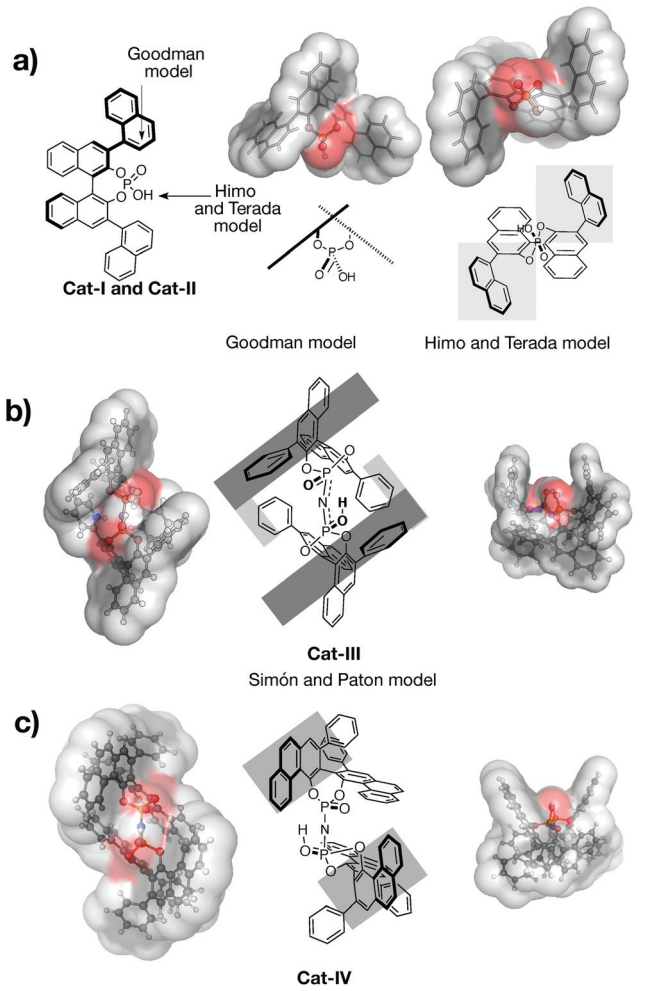

Fig. 3 (a) Projections of **Cat-I** and **Cat-II** for the Goodman and Himo and Terada models; (b) projection of **Cat-III** for the Simón and Paton model; (c) projection of **Cat-IV** for the Simón and Paton model. Gray boxes represent "hindered" regions of space.

the bottom (as it is more visible in the zenithal representation of the catalyst, Fig. 3c, right). It is also clear that the cavity is wider than in the case of **Cat-III**.

In all cases, after the suitable projection was chosen, application of these qualitative predicting guides consists of placement of the reagents in the catalyst cavity, identifying the position, orientation or conformation that lead the substituents toward the less hindered regions of the space. The ability of these models to explain (or predict) the stereochemical outcome of the reaction was studied by projecting the TS structures as in the models and comparing the calculated relative energies.

Table 1 shows a summary of the results obtained for the four catalysts and the ability of the different prediction guides to justify these results based on the identified steric effects. The success and failure of the predicting guides is also commented on, listing the exceptions and their explanation. The rate-determining step for each enantiomer is also included. Subsequent sections for each studied catalyst contains a more

Table 1 Summary of the results found for the four catalysts and their justification by qualitative predicting guides

Catalyst	Enantiomeric excess, % (exp. *vs.* calc.)	Rate-determining step	Preferred isomerization mechanism	Model for addition step	Model for isomerization step
Cat-I	93/94	Isomerization for both enantiomers	"Indole H-bonded" for *exo* intermediates, "tosylamide-H-bonded" for *endo* intermediates	*Endo* preferred. Explained by Goodman's model	Exceptions in some TS structures: – Energies of the Wheland intermediate conformations – H-bond with Tos NH (distorts H-bond with indole NH)
Cat-II	56/47	Isomerization for both enantiomers	"Tosylamide-H-bonded" for *R-endo* intermediate, "indole H-bonded" for the other intermediates	*Endo* preferred. Explained by Goodman's model	Exceptions in some TS structures: – Energies of the Wheland intermediate conformations – H-bond with Tos NH (distorts H-bond with indole NH) – Deviation from the model for Cat-I owing to the smaller catalyst cavity
Cat-III	91/90	Isomerization (*S* product), addition (*R* product)	"Indole H-bonded" in all cases	*Exo* preferred. Explained by Simón and Paton model	Predictable additional H-bond with Tos NH in most stable TSs (does not distort H-bond with indole NH) Exceptions due to conformation of the Wheland intermediate in some TSs
Cat IV	83/87	Addition for both enantiomers	"Indole H-bonded" in all cases	*Exo* preferred. Explained by Simón and Paton model	Conformation of the Wheland intermediate more relevant than additional H-bonds with Tos NH

detailed description of the results, including the energy diagram for the reaction, the proposed model for each step, and the rationalization of the calculated relative energies. The impossibility of using predicting guides to forecast the enantioselectivity of the reaction is explored next, discussing the difficulties of the models and showing examples of how different arguments are required to explain the TSs energies for different catalysts.

Reaction catalysed by Cat-I

The Friedel–Crafts reaction between indole and the *N*-tosylimide of benzaldehyde catalysed by **Cat-I** has already been studied by Simón and Goodman,[33] although the re-aromatization step was not explicitly considered. The mechanism is re-examined here to account for the re-aromatization step and to gain consistence with the methodology employed with other catalysts.

The energy diagram, including only the most stable TS structures, is shown in Fig. 4. For *R-endo*, *S-exo*, and *S-endo* pathways it was not possible to find any TSs for the isomerization step with lower energy than the energy of the addition step. Therefore, according to the Curtin–Hammet principle, the re-aromatization step is rate-determining for these paths. Using Maxwell–Boltzmann distribution and considering all TSs found for each stereo-determining step, 94% ee is calculated, in excellent agreement with the experimental result (93% ee). Interestingly, if only the addition step was considered, the results would have predicted an absolute configuration of the major product that does not correspond to the experimental observations.

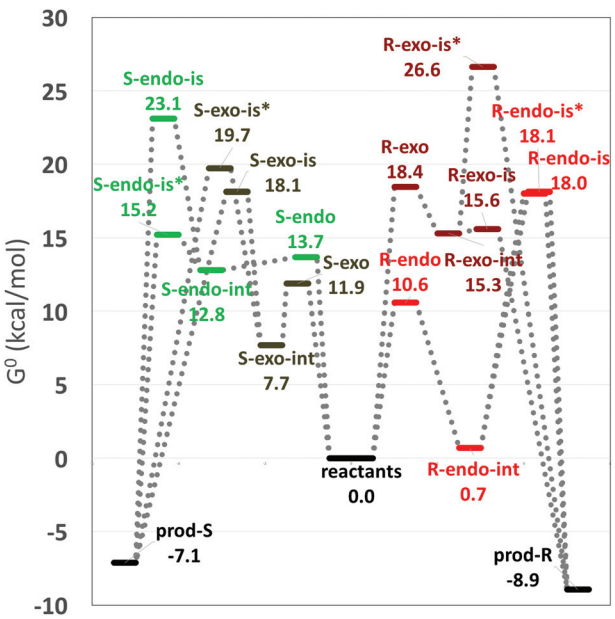

Fig. 4 Energy diagram for the Friedel–Crafts reaction catalysed by Cat I. TSs for "*indole H-bonded*" and "*tosylamide H-bonded*" re-aromatization mechanisms are labelled "-is" and "-is*", respectively.

In concordance with Simón and Goodman's results,[33] *endo* TSs are more stable than similar *exo* TSs. This was attributed to a better fit of the CPA phosphate to *endo* TSs: the distance between the catalyst's phosphate oxygen atoms (2.6 Å) is closer to the distance between nucleophile and electrophile N atoms

in *endo* TSs (3.2–3.3 Å) than in *exo* TSs (3.8–4.0 Å). However, in Simón and Goodman's work,[33] this ***R-endo*** TS showed a *gauche* conformation ("**C**" in Fig. 2d), while here the most stable TSs correspond to a lower energy *anti* ("**A**") conformation (in current calculations, "**C**" *R-endo* TS has also been found and its energy, 16.9 kcal mol^{-1}, is 6.3 kcal mol^{-1} higher than the TSs with the "**A**" conformation).

Goodman's[39] model can be used to prognosticate the energies of the addition step (Fig. 5): assuming that the most stable TSs should correspond to *endo* relative orientation of the reagents, the indole will preferentially place their C4, C5, C6, and C7 atoms in one of the vacant regions (to the right, if it is on the top), leading to the ***R-endo*** TSs (Fig. 5, top-left). The calculated relative energies agree with this model.

For the "*indole H-bonded*" mechanism, an attempt to employ the Himo–Terada[30,102] model was made. The C1′ atom can be placed in any of the two less hindered quadrants: the upper-left quadrant for TSs in the *R-exo* and *S-endo* paths (Fig. 6a, green model) and the lower-right quadrant in TSs in the *S-exo* and *R-endo* paths (Fig. 6a, pink model). The two possibilities are not equivalent, and TSs in the *S-exo* and *R-endo* the C1′ substituents are displaced toward the hindered upper-right quadrant. This should lead to less stable TSs for these two paths. In both cases, the larger substituent (the Ph group) would preferentially be perpendicular to the projection and away from the catalyst cavity, while the smaller group (the H atom) would be directed toward the closer catalyst side substituent (Fig. 6b).

Schematic representation of the "*indole H-Bond*" isomerization TSs and calculated energies are shown in Fig. 6c. In the most stable TSs (***R-exo*-Tos-A**) the optimum disposition of the smaller (H), medium (Tos) and large (Ph) groups, predicted by the model in Fig. 6b, is present. Owing to the change in the configuration of the C1′ carbon atom, the TSs in the *S-endo* paths is not able to achieve this arrangement. ***S-exo*-H** TSs also shows the more convenient arrangement of the C1′ substituents, but suffers the penalty of *S-exo* and *R-endo* TSs.

The stability of other TSs, however, does not emerge from the simple model. For ***S-exo*-Tos** TSs, there is an additional H-bond between the tosyl-NH and one phosphate oxygen (*d* O···H: 2.1 Å, although it distorts the H-bond between the indole NH and the phosphate: the O···H distance increased to 3 Å). This H-bond contributes to reduce the energy of the TSs. Also unexpectedly, ***R-endo*-H** TSs is less stable than ***R-endo*-Tos**

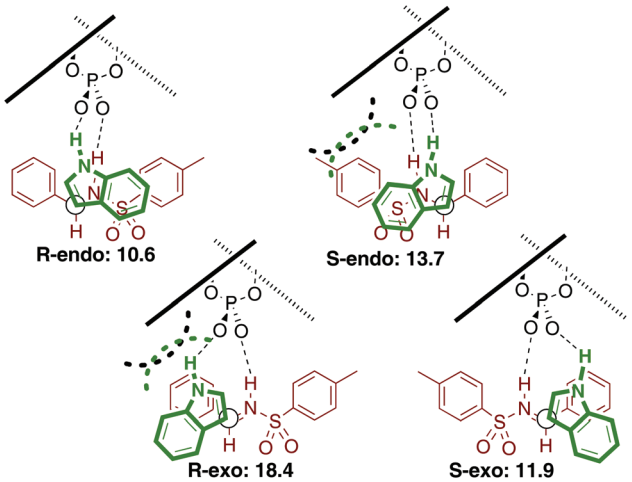

Fig. 5 Application of Goodman's model to the addition step of the reaction catalysed by **Cat I**, and calculated TSs energies (in kcal mol^{-1}).

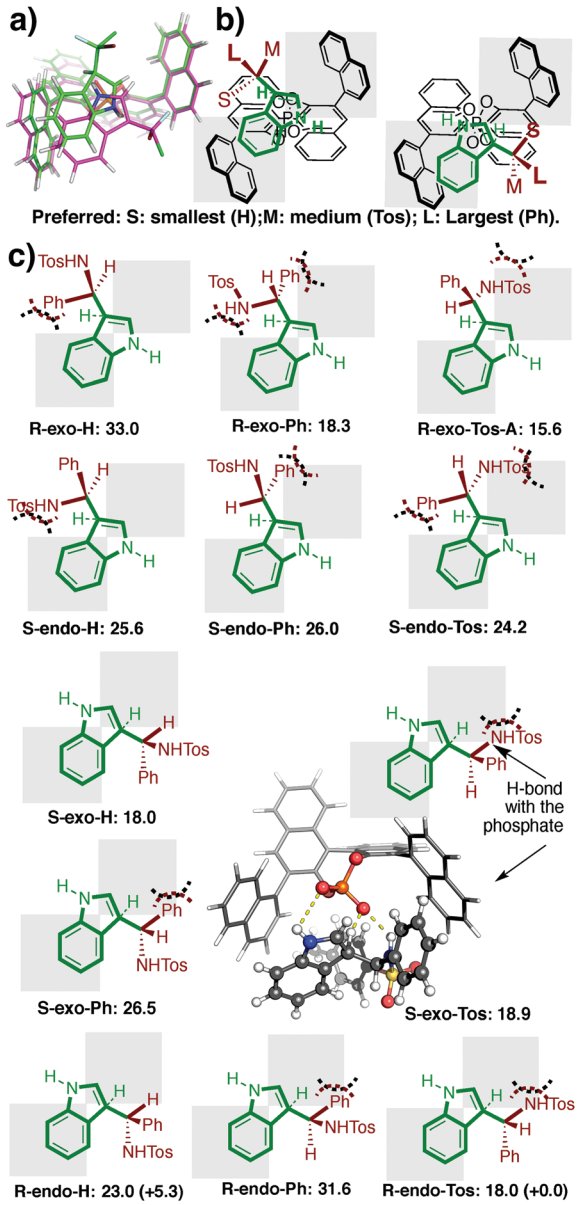

Fig. 6 (a) Overlay of the arrangement of the indole group in the catalyst cavity. (b) Model for minimizing steric interactions between the Wheland intermediate substituents and the catalyst. (c) TS structures found for the "*indole H-bonded*" isomerization step and their calculated energies (in kcal mol^{-1}). The relative energies of the conformations of the intermediate are included in parentheses. Gray boxes represent "hindered" quadrants.

TSs. The justification requires considering the relative energies of the conformation of the Wheland intermediate, which is particularly stable for ***R-endo*-Tos** TSs compared to ***R-endo*-H** TSs (shown in Fig. 6c in parentheses).

For the "*tosylimide H-bonded*" isomerization mechanism, the Himo–Terada[30,102] projection can also be used. The optimal location of the groups (Fig. 7) would place the larger Ph group preferentially in the position directed away from the catalyst cavity. Although this should be the case for the TSs in the *S-exo* and *R-exo* paths, a very unfavourable conformation of the Wheland intermediate yields a high energy TSs in the *S-exo* path and even prevents finding a TSs in the *R-exo* path (although failure to find this TSs does not affect the product distribution since in this reaction path the rate is determined during the addition step). The most stable TSs for this mechanism is ***S-endo*** TSs. The Ph group is parallel to the catalyst's left substituent, reducing the steric interactions that the model would have anticipated.

Reaction catalysed by Cat-II

The energy diagram for the reaction catalysed by the SPINOL-derived **Cat-II** is shown in Fig. 8a. Application of the Curtin–Hammet principle and Maxwell–Boltzmann averages to the TS structures found yields a 47% ee, in good agreement with the experimental results (56% ee). As for **Cat-I**, the only pathway that is controlled during the addition step is the *R-exo* route. Again, if only the addition step was considered, the calculations would not be able to predict the experimental results since a much larger degree of enantioselectivity will be expected.

Goodman's[39] model (Fig. 8c) can also be used to guess the stereoselectivity during the addition step. However, compared to BINOP CPAs, the cavity of SPINOL-derived CPA is smaller, conditioning the stability of some of the TSs. In particular, ***R-endo*** TSs is damaged by this reduction in the cavity: severe steric interactions with the catalysts preclude adopting the *anti*

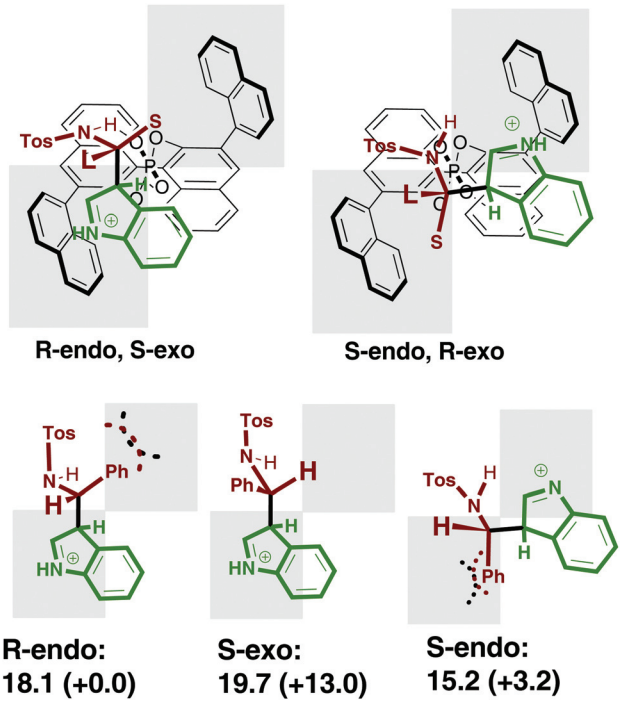

Fig. 7 Top: Models for minimizing the steric interactions between the catalyst and the intermediate in the ""*indole H-bonded*" re-aromatization TSs. Bottom: TSs found and calculated energies (in kcal mol^{-1}). Relative energies of the conformations of the intermediate are included in parentheses. Gray boxes represent "hindered" quadrants.

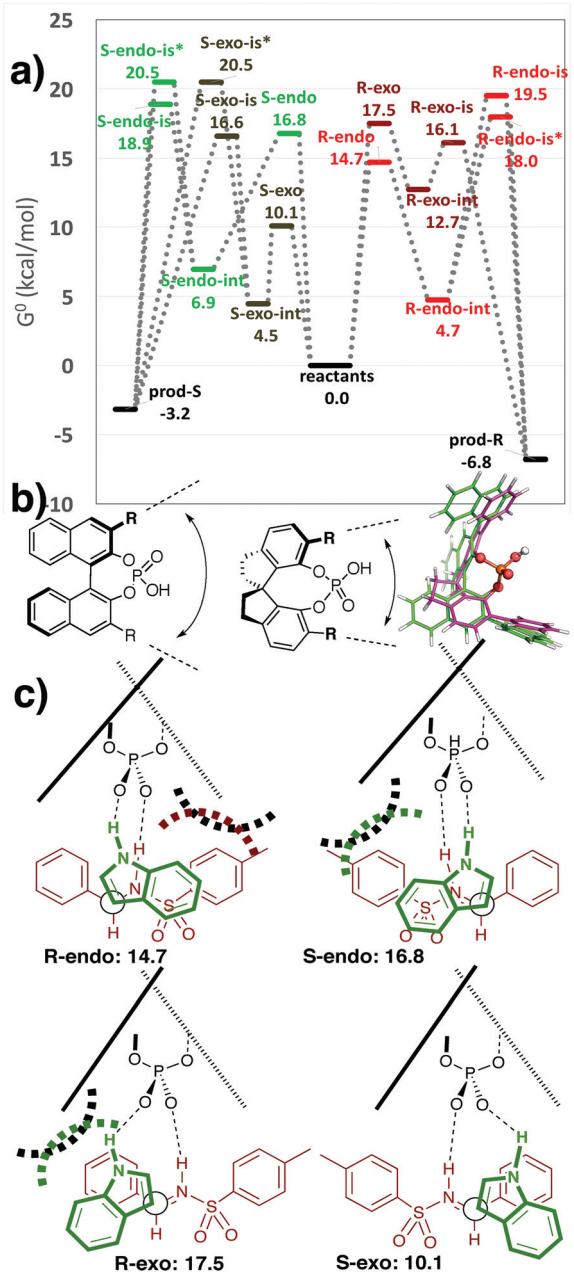

Fig. 8 (a) Energy diagram for the reaction catalysed by **Cat-II**. TSs for "*indole H-bonded*" and "*tosylamide H-bonded*" isomerization mechanisms are labelled "-is" and "-is*", respectively. (b) Comparison between the cavities of **Cat-I** and **Cat-II**; (c) Goodman model for the TSs of the addition reaction and energies (in kcal mol^{-1}) of the TSs found.

("**A**") conformation found for **Cat-I** and only the less stable *gauche* "**C**" conformation was found. As a consequence, the most stable addition TSs is no longer the ***R-endo*** TSs, but ***S-exo*** TSs (despite the *exo* disadvantage), for which preventing steric interactions with the catalysts is easier. This change in the preference was already predicted for other reactions by Jonathan and Reid making use of their model,[47,48] considering the change from a medium-sized cavity to a small cavity. The employment of this model, therefore, requires accepting a small cavity for SPINOL-derived CPA and a medium-sized cavity for 1-naphthyl-substituted BINOP, which could be difficult to anticipate without performing the calculations.

The Himo–Terada[30,102] projection can also offer a guide for predicting the relative energies of TSs for the "*indole H-bonded*" mechanism (Fig. 9a). When comparing with the calculated energies, a first observation is that the narrower cavity of the catalyst also has consequences during this step. For *R-exo* and *S-endo* TSs, steric interactions with the groups in the upper-right quadrant become more relevant than for **Cat-I**, and accordingly the advantage of the ***R-exo*-Tos** TSs is reduced. Additionally, the indole tilts and adopts a more "oblique" disposition (visible in the zenithal projection of the TSs, Fig. 8b). This change moves the Ph group outward in ***S-exo*-H** and ***R-endo*-H** TSs, increasing their stability, but pushes the tosyl group toward the top-right quadrant for ***S-exo*-Tos**, destabilizing it. Like in the case of **Cat-I**, ***S-exo*-Tos** TSs shows an additional H-bond between the phosphate oxygen and tosyl-imide NH (*d* O···H: 1.9 Å with tosyl-imide NH and 2.6–2.9 Å with indole N–H).

The narrower cavity affects the TSs for the "*tosylamide H-bonded*" isomerization mechanism as well and conditions the results that would have been extracted for the qualitative model (Fig. 10). Starting from the most stable TSs found for **Cat-I**, the tilt of the indole ring required in **Cat-II** would have pushed the Ph group toward the catalyst substituent at the left side. The consequences of this movement are so severe that this TSs has not even been found. Instead, an alternative TSs in which the Wheland intermediate shows a different and less stable conformation was obtained (Fig. 10, in parentheses). The large energy of the Wheland intermediate conformation is, like for **Cat-I**, the reason behind the impossibility of finding a TS structure for the **R-*exo*** path, and justifies the instability of ***S-exo*** TSs.

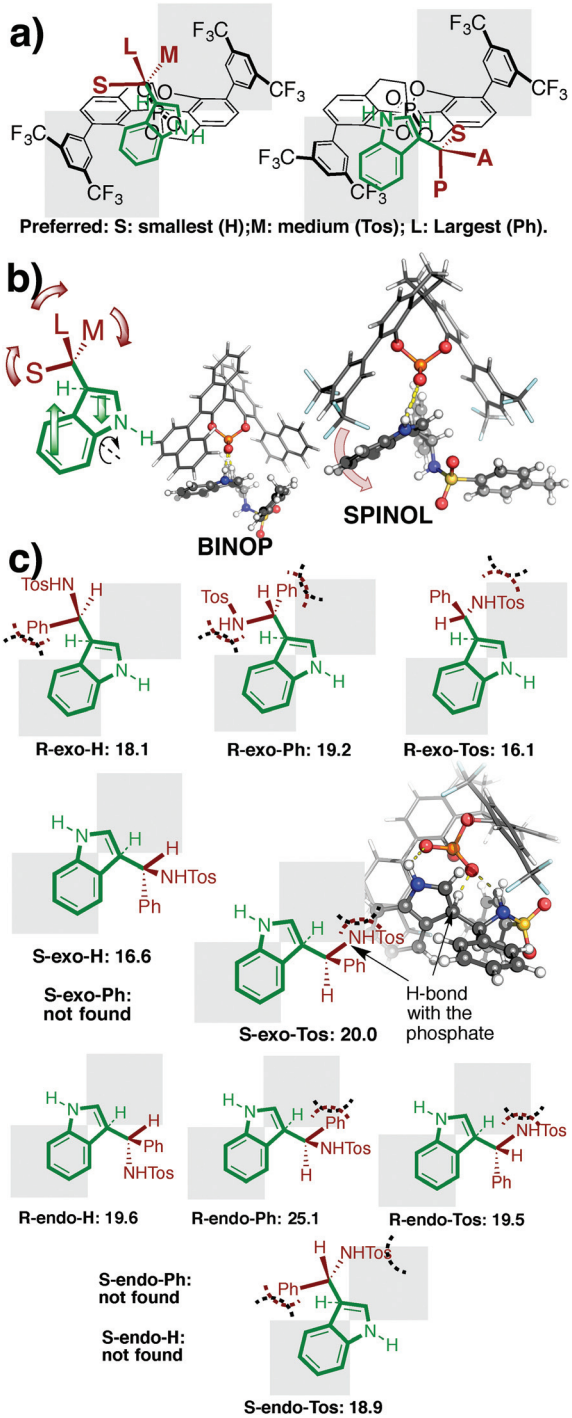

Fig. 9 (a) Model for the optimal arrangement of the intermediate substituents. (b) Tilt of the indole intermediate to fit in the reduced cavity of **Cat-II**. (c) TSs for the "*indol H-bonded*" isomerization mechanism. Energies are in kcal mol^{-1}. Gray boxes represent "hindered" quadrants.

Reaction catalysed by Cat-III

The energy diagram for the reaction catalyzed by **Cat-III** is shown in Fig. 11a. The TSs found and the application of the Curtin–Hammet principle offered a 91% ee of the *S* product, in excellent agreement with the experimental results (90% ee). The distance between the imidodiphosphoric oxygen atoms is 3.6–4.0 Å, implying that this catalyst is better suited for *exo* addition TSs (with a ≈4.0 Å distance between the nitrogen atoms in indole and tosylimine) than for *endo* TSs (3.1–3.3 Å). Accordingly, the most stable TS structures correspond to the *exo* addition pathway. With this catalyst, the rate-determining step is the addition, except for the *S-exo* route. **Cat-III** seems more appropriate for the re-aromatization step using the "*indole H-bonded*" mechanism. However, the stereochemistry of the product is reduced as a consequence of a limited effectiveness in assisting this step in the *S-exo* route. All TSs corresponding to the "*tosylamide H-bonded*" isomerization mecha-

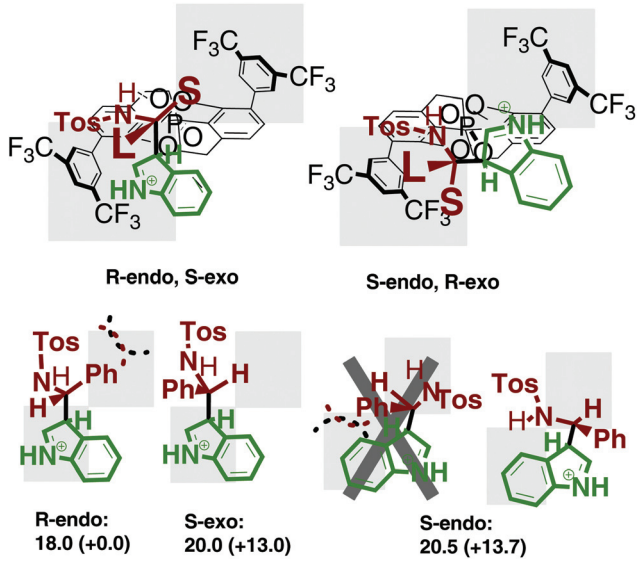

Fig. 10 Top: Model for the optimal arrangement of groups in "*tosylamide H-bonded*" isomerization TS structures for **Cat-II**. Bottom: TSs found. Energies are in kcal mol^{-1}. In parentheses, the energies of the conformation of the Wheland intermediate. Gray boxes represent "hindered" quadrants.

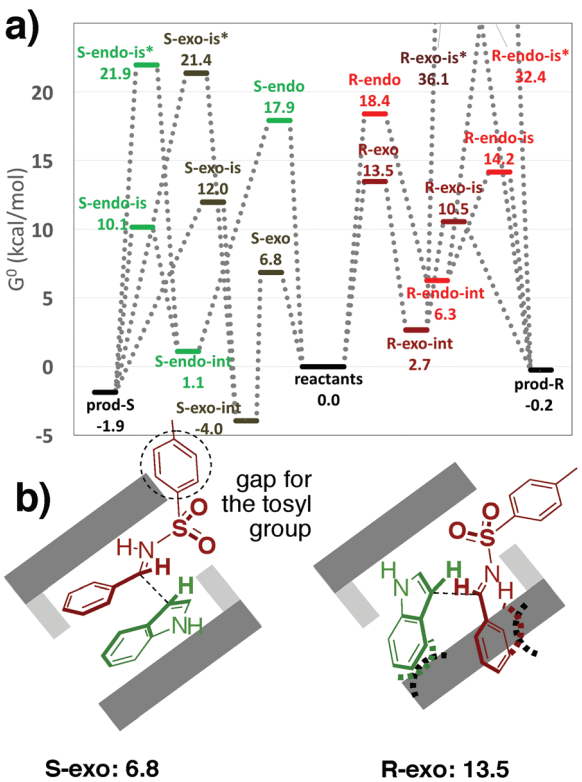

Fig. 11 (a) Energy diagram for the reaction catalysed by **Cat-III**. TSs for "*indole H-bonded*" and "*tosylamide H-bonded*" isomerization mechanisms are labelled "-is" and "-is*", respectively. (b) Frontal representation of the solvent-accessible surface of **Cat-III**. (c) Model for explaining the selectivity of the addition step. Energies are in kcal mol^{-1}. Gray boxes represent "hindered" regions of space.

nism have large energies, which can be explained by the incompatibility between the distance between imidodiphosphoric oxygen atoms (≈3.9 Å) and between the tosylamide NH and the H atom removed from C3 (≈2.7 Å).

The frontal representation proposed by Simón and Paton[85] shows, for the most stable *S-exo* addition TSs, the two reagents laid parallel to the cavity walls, and the tosyl group placed in the gap left between the side and top limiting Ph groups. In the anticipated less stable *R-exo* addition TSs, the imine phenyl group is directed toward the lower-right catalyst substituent. The results of the calculations show that this conjecture is correct.

The "Simón and Paton" representation can also considered as a guide for predicting the selectivity of the "*indole H-bonded*" isomerization TSs (Fig. 12).

For TSs in the *R-exo* and *S-endo* paths (Fig. 12, top) the C3–C1′ bond is parallel to the catalyst groove. The three substituents of C1′ can then be directed toward the phenyl side substituent at the top (dark-gray bar), the substituent at the bottom (light-gray bar) or outside of the catalyst cavity. The latter position is the only one that is not affected by steric interactions with the catalyst, and therefore would preferentially be occupied by the larger substituents. Indeed, the most stable TS structures (***S-endo*-H** and ***R-exo*-Tos**, Fig. 12, top) places the Ph group in this position, and TSs in which this position is occupied by the smaller H substituent have not even been found. In addition to the effect of steric interactions, the NH tosyl group in ***R-exo*-Tos** and ***S-endo*-H** can establish H-bonds with the imidodiphosphoric oxygen when it is not directed outward from the catalyst's cavity. Unlike in the cases of **Cat-I** and **Cat-II**, these additional H-bonds can be made without disturbing the H-bond with the indole NH. Formation of the additional H-bond is therefore very advantageous and, actually, TSs lacking this H-bond are not competitive. The model does not show a factor that could indicate a higher stability of any of the two TSs, ***R-exo*-Tos** or ***S-endo*-H**; confirming the model, the energy of both TSs is nearly identical (the very similar energies of the conformations also contribute to this result).

For "*indole H-bonded*" TSs in the *R-endo* and *S-exo* paths (Fig. 12, bottom), the C3–C1′ bond is perpendicular to the lower bound of the catalyst cavity, implying that these TSs have larger energies. One of the C1′ substituents is very near the catalyst's cavity wall, which should lead to important steric interactions unless it is the smaller substituent (the H atom). The other two substituents are less hindered, either because they are pointed outward from the catalyst's cavity, or are laid parallel to the cavity walls. There is also the possibility of additional H-bonds when this when this last substituent is the NH-Tos group. When this model is compared with the actual calculated energies, there are notable exceptions. For example, in ***S-exo*-Ph** (Fig. 12, bottom) TSs the most hindered position is occupied by the larger Ph group; to minimize steric interactions, in this TSs the C3–C1′ bond adopts an eclipsed conformation. But surprisingly, the energy of this TSs is smaller than the energy of ***R-endo*-H** TSs. In both cases the tosyl NH is able to make an additional H-bond with the catalyst, but the conformation of the Wheland intermediate in ***R-endo*-H** is particularly unstable.

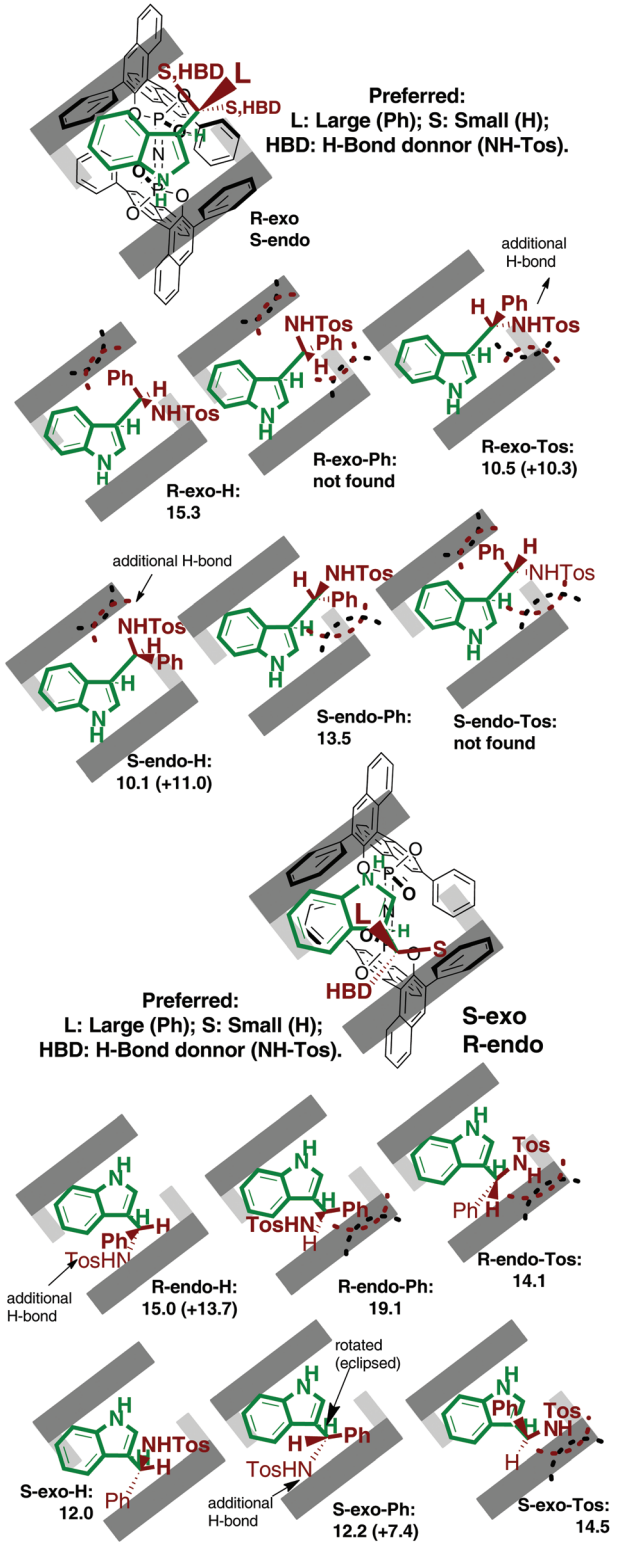

Fig. 12 Model to justify the relative energies of the "*indole H-bonded*" isomerization TSs and the TSs found for **Cat-III**. Energies are in kcal mol^{-1}. In parentheses, the energies of the conformation of the Wheland intermediate. Gray boxes represent "hindered" regions of space.

Reaction catalysed by Cat-IV

There are several similarities between the mechanism of the reactions catalysed by **Cat-III** and **Cat-IV**. The energy of *endo* addition TSs is higher than *exo* TSs (energy diagram in Fig. 13; since their energy is also much higher than any TS structures in the *exo* pathways, *endo* paths do not contribute to the final product stereoselectivity, and isomerization TSs were not searched). The TSs of the energies of "*indole H-bonded*" mechanism are more stable than the TSs of the addition step, while the TSs of "*tosylamide H-bonded*" re-aromatization have a very high energy. The isomerization step is not stereo-determining and does not reduce the degree of selectivity obtained during the addition step. Accordingly, although the addition step is less selective for **Cat-IV** than for **Cat-III**, the enantiomeric excesses offered by the two catalysts are similar. The calculated enantiomeric excess for this reaction, 87% ee, compares well with the experimental value, 83% ee.

The frontal representation can also serve to formulate a guide for predicting the selectivity in both reaction steps. For the addition step, the same arguments used for **Cat-III** can also be employed here, but in agreement with the wider and less sterically demanding cavity, the calculated energy difference between the two addition TSs is reduced.

For the "*indole H-bonded*" TSs, the energies of the TSs do not fit well into a similar model to **Cat-III** (Fig. 14). It is evident that the relative stability of the conformation is more relevant than the possibility of establishing additional

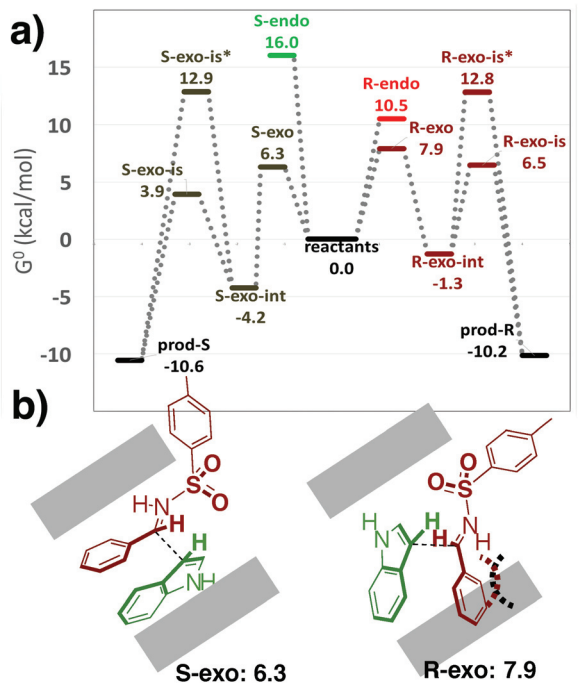

Fig. 13 (a) Energy diagram for the reaction catalysed by **Cat-IV**; TSs for "*indole H-bonded*" and "*tosylamide H-bonded*" isomerization mechanisms are labelled "-is" and "-is*", respectively. (b) Model explaining the selectivity of the addition step. Energies are in kcal mol^{-1}. Gray boxes represent "hindered" regions of space.

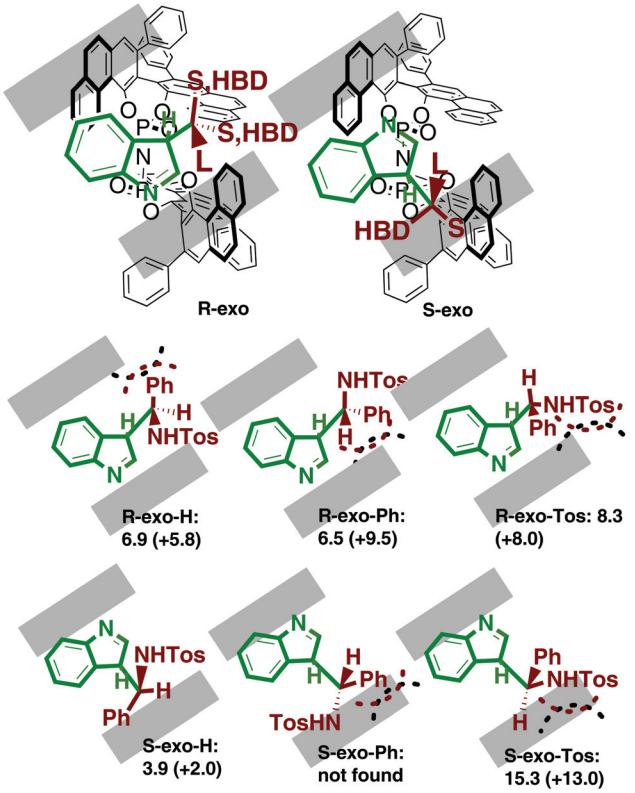

Fig. 14 Model to justify the relative energies of the *"indole H-bonded"* TSs and the TSs found for **Cat-IV**. Energies are in kcal mol^{-1}. In parentheses, the energies of the conformation of the Wheland intermediate. Gray boxes represent "hindered" regions of space.

H-bonds. For example, ***R-exo*-H** TSs neither poses the largest Ph group outward from the catalyst cavity nor affords an additional H-bond with the NH-Tos group, but the Wheland intermediate adopts a more stable conformation. This fact alone justifies its relatively lower energy. The wider cavity also reduces the penalty of TSs in the *S-exo* route. Actually, the most stable TSs for the "*indole H-Bonded*" mechanism is ***S-exo*-H**; it is also not able to make the additional H-bond with the tosylamide but has a very stable conformation. In this TSs the H atom occupies the most hindered position. Attempts to place any of the other two groups in this position lead to a large energy (***S-exo*-Tos** TSs) or even to the impossibility of finding the corresponding TSs (***S-exo*-Ph**).

Can a qualitative model predict these results?

Despite the necessity of contemplating different conformations and relative orientations of the reactants and different reaction steps, once the TSs are found the factors that contribute to their energy can be easily identified: steric interactions, the possibility of establishing additional H-bonds, and the relative energy of the conformation of the intermediate in the TSs. However, although the mode of activation is not different to other theoretically studied CPA-catalysed reactions, the employment of a guide derived from these reactions to predict the stereochemical outcome of the reaction, without performing any calculation, has some problems:

First, the reaction consists of two consecutive (and competitive) steps. The relevance of the second step varies with the catalysts: it reverses the enantioselectivity in the case of **Cat-I** with respect to what would be expected from the addition step, reduces the degree of enantioselectivity for **Cat-II** and **Cat-III**, and is irrelevant for **Cat-IV**. Some of the observations for the relative energies of TSs for the addition and re-aromatization step could be anticipated in a model. For example, the high energy of "*tosylamide H-bonded*" rearomatization TSs for **Cat-III** and **Cat IV** could have been prognosticated from the different distance between the imidodiphosphoric oxygens and the substrate H atoms. However, it is not so obvious why, for example, "*indole H-bonded*" TSs have smaller energies than addition TSs in the case of **Cat-IV** but not in the related **Cat-III**.

Second, small differences in the catalyst in some cases lead to very different behaviour. Goodman's model predicts, to some extent, the effect of the size of the cavity on the change of the preference for *R-endo* or *S-exo* addition TSs from **Cat-I** to **Cat-II**. However, establishing when the cavity can be considered medium-sized or small, to apply one model or the other, is more difficult. For the "*tosylamide H-bonded*" isomerization mechanism, the ***S-endo*** TSs "just fits" in the cavity of **Cat-I**, but severe steric interactions prevented even obtaining the corresponding TSs for **Cat-II**.

Finally, the balance between the three factors that are identified to contribute to the energies of the TSs (steric interactions, additional H-bonds and relative energy of the conformations) is not obvious even for similar catalysts. For example, for the "*indole H-bonded*" re-aromatization the possibility of establishing an additional H-bond is very important to yield low-energy TSs in the case of **Cat-III**, but for **Cat-IV** the relative energy of the conformation has a stronger influence.

The difficulties in deducing and applying a valid qualitative model as a guide for this reaction should not be interpreted neither as a failure of these models nor against the ambition of their creators. The overwhelming validity of some of these models (for example, Goodman's models are legitimated against reactions from more than 40[38] or 70[48] literature references) confirms that the Friedel–Crafts reaction studied here constitutes an exception. However, other reactions consisting of several competitive steps, with a large degree of flexibility for reagent conformation and orientation, and with the possibility of building up additional interactions, can also impose difficulties at the moment of finding these guides. In these cases, qualitative models cannot replace the theoretical study of the reaction mechanism. Methodologies for automatic exploration of the conformational space and the different steps of the reaction are, therefore, of crucial interest.[103–109]

Conclusions

The mechanism of the Friedel–Crafts reaction between tosyimide of benzaldehyde and indole catalysed by CPA catalysts

has been investigated by ONIOM QM/MM methods. The fact that the experimental enantioselectivities can only be reproduced when the re-aromatization step is taken into account confirms the relevance of the catalyst in assisting during this second step. Indeed, for the BINOP-derived CPA the re-aromatization step changes the sense of the enantioselectivity; for SPINOL-derived CPA or the BINOP-derived imidodiphosphoric acid the re-aromatization step reduces the selectivity, and for the VAPOL-derived imidodiphosphoric acid it is irrelevant. Predicting the influence of the isomerization step on the reaction selectivity is not possible without the help of calculations.

The relative energies of TSs corresponding to the same reaction step can be rationalized in most cases making use of the steric interactions with the catalyst. The preference of *endo* and *exo* addition TS structures can also be justified based on the distance between the CPA oxygen atoms. This is also the case of the inappropriate geometry of imidodiphosphate catalysts to assist in the "*tosylimide H-bonded*" re-aromatization mechanism. Nevertheless, there are also notable exceptions in which rationalization requires more elaborate arguments, such as additional H-bond interactions or the presence of particularly unstable conformations on the reagents. The relevance and arbitrary occurrence of these secondary factors makes the use of guides for predicting the stereoselectivity difficult in this particular reaction.

Conflicts of interest

There are no conflicts to declare.

Acknowledgements

I thank Prof. Robert S. Paton for fruitful discussion and for suggesting the possibility of the "*tosylamide H-bonded*" re-aromatization mechanism. Financial support from the University of Salamanca (18.K114) is acknowledged. I thank A. Lopez García and J. A. González Ramos for IT support, and the University of Salamanca server housing service.

Notes and references

1 L. Simón and J. M. Goodman, *Org. Biomol. Chem.*, 2011, **9**, 689–700.
2 R. Peverati and D. G. Truhlar, *Philos. Trans. R. Soc., A*, 2014, **372**, 20120476.
3 S. Grimme, A. Hansen, J. G. Brandenburg and C. Bannwarth, *Chem. Rev.*, 2016, **116**, 5105–5154.
4 D. J. Tantillo, *Acc. Chem. Res.*, 2016, **49**, 1079.
5 Q. Peng, F. Duarte and R. S. Paton, *Chem. Soc. Rev.*, 2016, **45**, 6093–6107.
6 Y. H. Lam, M. N. Grayson, M. C. Holland, A. Simon and K. N. Houk, *Acc. Chem. Res.*, 2016, **49**, 750–762.
7 P. H. Cheong, C. Y. Legault, J. M. Um, N. Celebi-Olcum and K. N. Houk, *Chem. Rev.*, 2011, **111**, 5042–5137.
8 S. Bahmanyar, K. N. Houk, H. J. Martin and B. List, *J. Am. Chem. Soc.*, 2003, **125**, 2475–2479.
9 S. Bahmanyar and K. N. Houk, *Org. Lett.*, 2003, **5**, 1249–1251.
10 F. R. Clemente and K. N. Houk, *J. Am. Chem. Soc.*, 2005, **127**, 11294–11302.
11 J. Franzen, M. Marigo, D. Fielenbach, T. C. Wabnitz, A. Kjarsgaard and K. A. Jorgensen, *J. Am. Chem. Soc.*, 2005, **127**, 18296–18304.
12 A. Hamza, G. Schubert, T. Soos and I. Papai, *J. Am. Chem. Soc.*, 2006, **128**, 13151–13160.
13 B. Kótai, G. Kardos, A. Hamza, V. Farkas, I. Pápai and T. Soós, *Chem. – Eur. J.*, 2014, **20**, 5631–5639.
14 M. N. Grayson and K. N. Houk, *J. Am. Chem. Soc.*, 2016, **138**, 1170–1173.
15 M. Li, X.-S. Xue and J.-P. Cheng, *ACS Catal.*, 2017, **7**, 7977–7986.
16 M. N. Grayson and K. N. Houk, *J. Am. Chem. Soc.*, 2016, **138**, 9041–9044.
17 J. Guo and M. W. Wong, *J. Org. Chem.*, 2017, **82**, 4362–4368.
18 X. Zhang, H. Du, Z. Wang, Y. D. Wu and K. Ding, *J. Org. Chem.*, 2006, **71**, 2862–2869.
19 A. Zamfir, S. Schenker, M. Freund and S. B. Tsogoeva, *Org. Biomol. Chem.*, 2010, **8**, 5262–5276.
20 M. Rueping, A. Kuenkel and I. Atodiresei, *Chem. Soc. Rev.*, 2011, **40**, 4539–4549.
21 S. Schenker, A. Zamfir, M. Freund and S. B. Tsogoeva, *Eur. J. Org. Chem.*, 2011, 2209–2222.
22 D. Parmar, E. Sugiono, S. Raja and M. Rueping, *Chem. Rev.*, 2014, **114**, 9047–9153.
23 M. Terada, *Chem. Commun.*, 2008, **2008**, 4097–4112.
24 G. Adair, S. Mukherjee and B. List, *Aldrichimica Acta*, 2008, **41**, 31–39.
25 M. Rueping, R. M. Koenigs and I. Atodiresei, *Chem. – Eur. J.*, 2010, **16**, 9350–9365.
26 J. Yu, F. Shi and L.-Z. Gong, *Acc. Chem. Res.*, 2011, **44**, 1156–1171.
27 T. Akiyama, *Chem. Rev.*, 2007, **107**, 5744–5758.
28 S.-L. You, *Chem. – Asian J.*, 2007, **2**, 820–827.
29 L. Simón and J. M. Goodman, *J. Am. Chem. Soc.*, 2008, **130**, 8741–8747.
30 T. Marcelli, P. Hammar and F. Himo, *Chem. – Eur. J.*, 2008, **14**, 8562–8571.
31 T. Marcelli, P. Hammar and F. Himo, *Adv. Synth. Catal.*, 2009, **351**, 525–529.
32 L. Simón and J. M. Goodman, *J. Am. Chem. Soc.*, 2009, **131**, 4070–4077.
33 L. Simón and J. M. Goodman, *J. Org. Chem.*, 2010, **75**, 589–597.
34 F.-Q. Shi and B.-A. Song, *Org. Biomol. Chem.*, 2009, **7**, 1292–1298.
35 T. Akiyama, H. Morita, P. Bachu, K. Mori, M. Yamanaka and T. Hirata, *Tetrahedron*, 2009, **65**, 4950–4956.
36 N. Li, X.-H. Chen, J. Song, S.-W. Luo, W. Fan and L.-Z. Gong, *J. Am. Chem. Soc.*, 2009, **131**, 15301–15310.

37 C. Zheng, Y.-F. Sheng, Y.-X. Li and S.-L. You, *Tetrahedron*, 2010, **66**, 2875–2880.
38 L. Simón and J. M. Goodman, *J. Org. Chem.*, 2011, **76**, 1775–1788.
39 J. P. Reid, L. Simón and J. M. Goodman, *Acc. Chem. Res.*, 2016, **49**, 1029–1041.
40 R. Maji, P. A. Champagne, K. N. Houk and S. E. Wheeler, *ACS Catal.*, 2017, **7**, 7332–7339.
41 K. Saito, K. Horiguchi, Y. Shibata, M. Yamanaka and T. Akiyama, *Chem. – Eur. J.*, 2014, **20**, 7616–7620.
42 K. Saito, Y. Shibata, M. Yamanaka and T. Akiyama, *J. Am. Chem. Soc.*, 2013, **135**, 11740–11743.
43 Y. Shibata and M. Yamanaka, *J. Org. Chem.*, 2013, **78**, 3731–3736.
44 R. B. Sunoj, *Acc. Chem. Res.*, 2016, **49**, 1019–1028.
45 Y. Y. Khomutnyk, A. J. Arguelles, G. A. Winschel, Z. Sun, P. M. Zimmerman and P. Nagorny, *J. Am. Chem. Soc.*, 2015, **138**, 444–456.
46 I. D. Gridnev, M. Kouchi, K. Sorimachi and M. Terada, *Tetrahedron Lett.*, 2007, **48**, 497–500.
47 J. P. Reid and J. M. Goodman, *J. Am. Chem. Soc.*, 2016, **138**, 7910–7917.
48 J. P. Reid and J. M. Goodman, *Chem. – Eur. J.*, 2017, **23**, 14248–14260.
49 M. Orlandi, F. D. Toste and M. S. Sigman, *Angew. Chem., Int. Ed.*, 2017, **56**, 14080–14084.
50 R. Dalpozzo, *Chem. Soc. Rev.*, 2015, **44**, 742–778.
51 Y. Li, C. Q. He, F. X. Gao, Z. Li, X. S. Xue, X. Li, K. N. Houk and J. P. Cheng, *Org. Lett.*, 2017, **19**, 1926–1929.
52 L. Y. Chen, H. He, W. H. Chan and A. W. Lee, *J. Org. Chem.*, 2011, **76**, 7141–7147.
53 Y. Qian, G. Ma, A. Lv, H.-L. Zhu, J. Zhao and V. H. Rawal, *Chem. Commun.*, 2010, **46**, 3004–3006.
54 B. L. Wang, N. K. Li, J. X. Zhang, G. G. Liu, T. Liu, Q. Shen and X. W. Wang, *Org. Biomol. Chem.*, 2011, **9**, 2614–2617.
55 P. Kumari, P. K. Bera, N.-U. H. Khan, R. I. Kureshy, S. H. R. Abdi and H. C. Bajaj, *Catal. Sci. Technol.*, 2014, **4**, 563–568.
56 L. Wang, A. Rahman and X. Lin, *Org. Biomol. Chem.*, 2017, **15**, 6033–6041.
57 J. T. M. Correia, B. List and F. Coelho, *Angew. Chem., Int. Ed.*, 2017, **56**, 7967–7970.
58 Y. Zhou, Z. L. Xia, Q. Gu and S. L. You, *Org. Lett.*, 2017, **19**, 762–765.
59 C. Garcia-Garcia, L. Ortiz-Rojano, S. Alvarez, R. Alvarez, M. Ribagorda and M. C. Carreno, *Org. Lett.*, 2016, **18**, 2224–2227.
60 G. Li, H. Liu, Y. Wang, S. Zhang, S. Lai, L. Tang, J. Zhao and Z. Tang, *Chem. Commun.*, 2016, **52**, 2304–2306.
61 S. Romanini, E. Galletti, L. Caruana, A. Mazzanti, F. Himo, S. Santoro, M. Fochi and L. Bernardi, *Chem. – Eur. J.*, 2015, **21**, 17578–17582.
62 B. Bi, Q.-X. Lou, Y.-Y. Ding, S.-W. Chen, S.-S. Zhang, W.-H. Hu and J.-L. Zhao, *Org. Lett.*, 2015, **17**, 540–543.
63 S. Qi, C.-Y. Liu, J.-Y. Ding and F.-S. Han, *Chem. Commun.*, 2014, **50**, 8605–8608.
64 S.-G. Wang, L. Han, M. Zeng, F.-L. Sun, W. Zhang and S.-L. You, *Org. Biomol. Chem.*, 2012, **10**, 3202–3209.
65 G.-W. Zhang, L. Wang, J. Nie and J.-A. Ma, *Adv. Synth. Catal.*, 2008, **350**, 1457–1463.
66 S.-G. Wang, W. Zhang and S.-L. You, *Org. Lett.*, 2013, **15**, 1488–1491.
67 M. Zheng, Y. Liu, C. Wang, S. Liu and W. Lin, *Chem. Sci.*, 2012, **3**, 2623–2627.
68 D. Enders, M. Ludwig and G. Raabe, *Chirality*, 2012, **24**, 215–222.
69 K. Wu, Y.-J. Jiang, Y.-S. Fan, D. Sha and S. Zhang, *Chem. – Eur. J.*, 2013, **19**, 474–478.
70 Q. Kang, Z.-A. Zhao and S.-L. You, *J. Am. Chem. Soc.*, 2007, **129**, 1484–1485.
71 F. Xu, D. Huang, C. Han, W. Shen, X. Lin and Y. Wang, *J. Org. Chem.*, 2010, **75**, 8677–8680.
72 C.-H. Xing, Y.-X. Liao, J. Ng and Q.-S. Hu, *J. Org. Chem.*, 2011, **76**, 4125–4131.
73 Q. Kang, Z.-A. Zhao and S.-L. You, *Tetrahedron*, 2009, **65**, 1603–1607.
74 M. Terada and K. Sorimachi, *J. Am. Chem. Soc.*, 2007, **129**, 292–293.
75 Y.-X. Jia, J. Zhong, S.-F. Zhu, C.-M. Zhang and Q.-L. Zhou, *Angew. Chem., Int. Ed.*, 2007, **46**, 5565–5567.
76 I. Mendez, R. Rodriguez, V. Polo, V. Passarelli, F. J. Lahoz, P. Garcia-Orduna and D. Carmona, *Chemistry*, 2016, **22**, 11064–11083.
77 Y.-Q. Wang, J. Song, R. Hong, H. Li and L. Deng, *J. Am. Chem. Soc.*, 2006, **128**, 8156–8157.
78 M. J. Frisch, *et al.*, *Gaussian 09, Revision B.01*, Gaussian, Inc., Wallingford CT, 2009.
79 S. Dapprich, I. Komáromi, K. S. Byun, K. Morokuma and M. J. Frisch, *J. Mol. Struct.*, 1999, **461**, 1–21.
80 T. Vreven and K. Morokuma, *J. Comput. Chem.*, 2000, **21**, 1419–1432.
81 L. W. Chung, W. M. Sameera, R. Ramozzi, A. J. Page, M. Hatanaka, G. P. Petrova, T. V. Harris, X. Li, Z. Ke, F. Liu, H. B. Li, L. Ding and K. Morokuma, *Chem. Rev.*, 2015, **115**, 5678–5796.
82 L. Simón and J. M. Goodman, *Org. Biomol. Chem.*, 2009, **7**, 483–487.
83 L. Simón and J. M. Goodman, *J. Am. Chem. Soc.*, 2012, **134**, 16869–16876.
84 L. Simón and R. S. Paton, *J. Org. Chem.*, 2015, **80**, 2756–2766.
85 L. Simón and R. S. Paton, *Org. Biomol. Chem.*, 2016, **14**, 3031–3039.
86 L. Simon and R. S. Paton, *J. Org. Chem.*, 2017, **82**, 3855–3863.
87 M. N. Grayson, S. C. Pellegrinet and J. M. Goodman, *J. Am. Chem. Soc.*, 2012, **134**, 2716–2722.
88 *The PyMOL Molecular Graphics System, Version 1.3*, Schrödinger, LLC, 2009–2010.
89 R. Krishnan, J. S. Binkley, R. Seeger and J. A. Pople, *J. Chem. Phys.*, 1980, **72**, 650–654.

90 P. M. W. Gill, B. G. Johnson, J. A. Pople and M. J. Frisch, *Chem. Phys. Lett.*, 1992, **197**, 499–505.
91 A. K. Rappé, C. J. Casewit, K. S. Colwell, W. A. Goddard III and W. M. Skid, *J. Am. Chem. Soc.*, 1992, **114**, 10024–10035.
92 J.-D. Chai and M. Head-Gordon, *Phys. Chem. Chem. Phys.*, 2008, **10**, 6615–6620.
93 R. Cammi, B. Mennucci and J. Tomasi, *J. Phys. Chem. A*, 1999, **103**, 9100–9108.
94 R. Cammi, B. Mennucci and J. Tomasi, *J. Phys. Chem. A*, 2000, **104**, 5631–5637.
95 M. Cossi, N. Rega, M. Scalmani and V. Barone, *J. Chem. Phys.*, 2001, **114**, 5691–5701.
96 M. Cossi, G. Scalmani, N. Rega and V. Barone, *J. Chem. Phys.*, 2002, **117**, 43–54.
97 M. Cossi, G. Scalmani, N. Rega and V. Barone, *J. Comput. Chem.*, 2003, **24**, 669–681.
98 A. V. Marenich, C. J. Cramer and D. G. Truhlar, *J. Phys. Chem. B*, 2009, **113**, 6378–6396.
99 S. Grimme, *Chem. – Eur. J.*, 2012, **18**, 9955–9964.
100 GoodVibes v2.0.1, I. Funes-Adois and R. Paton, 2017, https://github.com/bobbypaton/GoodVibes.
101 http://cccbdb.nist.gov.
102 M. Terada, K. Machioka and K. Sorimachi, *J. Am. Chem. Soc.*, 2007, **129**, 10336–10337.
103 S. E. Wheeler, T. J. Seguin, Y. Guan and A. C. Doney, *Acc. Chem. Res.*, 2016, **49**, 1061–1069.
104 A. C. Doney, B. J. Rooks, T. Lu and S. E. Wheeler, *ACS Catal.*, 2016, **6**, 7948–7955.
105 Y. Guan and S. E. Wheeler, *Angew. Chem., Int. Ed.*, 2017, **56**, 9101–9105.
106 E. Hansen, A. R. Rosales, B. Tutkowski, P. O. Norrby and O. Wiest, *Acc. Chem. Res.*, 2016, **49**, 996–1005.
107 J. M. Lee, X. Zhang, P. O. Norrby, P. Helquist and O. Wiest, *J. Org. Chem.*, 2016, **81**, 5314–5321.
108 A. Madarasz, D. Berta and R. S. Paton, *J. Chem. Theory Comput.*, 2016, **12**, 1833–1844.
109 W. M. Sameera, S. Maeda and K. Morokuma, *Acc. Chem. Res.*, 2016, **49**, 763–773.